Original Article

JCBFM

Journal of Cerebral Blood Flow & Metabolism
2023, Vol. 43(3) 460–475

DOI: 10.1177/0271678X221139084
journals.sagepub.com/home/jcbfm


Capillary transit time heterogeneity inhibits cerebral oxygen metabolism in patients with reduced cerebrovascular reserve capacity from steno-occlusive disease

Mark B Vestergaard[1], Helle K Iversen[2,3], Sofie Amalie Simonsen[2], Ulrich Lindberg[1], Stig P Cramer[1], Ulrik B Andersen[4] and Henrik BW Larsson[1,3]

Abstract

The healthy cerebral perfusion demonstrates a homogenous distribution of capillary transit times. A disruption of this homogeneity may inhibit the extraction of oxygen. A high degree of capillary transit time heterogeneity (CTH) describes that some capillaries have very low blood flows, while others have excessively high blood flows and consequently short transit times. Very short transit times could hinder the oxygen extraction due to insufficient time for diffusion of oxygen into the tissue. CTH could be a consequence of cerebral vessel disease. We examined whether patients with cerebral steno-occlusive vessel disease demonstrate high CTH and if elevation of cerebral blood flow (CBF) by administration of acetazolamide (ACZ) increases the cerebral metabolic rate of oxygen ($CMRO_2$), or if some patients demonstrate reduced $CMRO_2$ related to detrimental CTH. Thirty-four patients and thirty-one healthy controls participated. Global CBF and $CMRO_2$ were acquired using phase-contrast MRI. Regional brain maps of CTH were acquired using dynamic contrast-enhanced MRI. Patients with impaired cerebrovascular reserve capacity demonstrated elevated CTH and a significant reduction of $CMRO_2$ after administration of ACZ, which could be related to high CTH. Impaired oxygen extraction from CTH could be a contributing part of the declining brain health observed in patients with cerebral vessel disease.

Keywords

Cerebral blood flow, cerebral hemodynamics, cerebrovascular disease, oxygen extraction fraction (OEF), small vessel disease

Received 21 March 2022; Revised 31 August 2022; Accepted 6 October 2022

Introduction

Pre-cerebral and cerebral artery stenosis and occlusion can cause severe neurological symptoms and increase the risk for stroke and neurodegenerative disease.[1–6] Severe stenosis or occlusion reduce cerebral blood flow (CBF), cerebral perfusion pressure and cerebral hemodynamic in the regions of the brain supplied by the affected arteries. In early disease stages the impaired perfusion is counteracted by increasing the arteriovenous oxygen extraction ($A\text{-}V.O_2$) in order to maintain adequate cerebral metabolic rate of oxygen ($CMRO_2$), but over time the oxygen metabolism is

[1]Functional Imaging Unit, Department of Clinical Physiology and Nuclear Medicine, Copenhagen University Hospital Rigshospitalet, Glostrup, Denmark
[2]Department of Neurology, Copenhagen University Hospital Rigshospitalet, Glostrup, Denmark
[3]Department of Clinical Medicine, Faculty of Health and Medical Science, University of Copenhagen, Copenhagen, Denmark
[4]Department of Clinical Physiology and Nuclear Medicine, Copenhagen University Hospital Rigshospitalet, Glostrup, Denmark

Corresponding author:
Mark B Vestergaard, Department of Clinical Physiology and Nuclear Medicine, Rigshospitalet, Valdemar Hansens Vej 1-23, 2600 Glostrup, Denmark.
Email: mark.bitsch.vestergaard@regionh.dk

also reduced in the affected brain regions.[7] Reduced CBF and increased A-V.O_2 correlate with increased risk of stroke.[2,3,8] In addition to reduced resting CBF, the cerebrovascular reserve capacity (CVR) induced by vasodilation stimulation may also be impaired, which similarly is associated with significant higher risks of stroke and neurodegenerative disease.[4–6,9–11]

Normalizing CBF and CVR by carotid endarterectomy or carotid angioplasty has demonstrated mixed results where some patients improve the oxygen metabolism but other patients have no effect, indicating that normalizing CBF may not necessarily translate to higher oxygen metabolism.[12–14] A possible reason for a missing improvement could be due to disruption of the microperfusion from cerebral vessel disease resulting in an uneven distribution of blood flow and transit times in the capillaries, a phenomenon called capillary transit time heterogeneity (CTH).[15–18] A high CTH describes that in some capillaries the blood flow is inadequately low and with long transit times, whereas other capillaries have very high blood flows and consequently short transit times. Short transit times will reduce the oxygen extraction fraction as there is less time for the oxygen to diffuse into the surrounding tissue, as described by the Crone-Renkin single capillary flow-diffusion model.[19] Thus, in situations with high CTH, both the low perfusion in some capillaries and very high perfusion in other capillaries could have a negative effect on the oxygen delivery to the tissue. High CTH impairing the cerebral oxygen metabolism has been suggested as a disease mechanism and could potentially play a causal role in the development of neurodegenerative disease.[20–23] A high CTH could lower the oxygen availability to the brain tissue, which then could reach a level below the metabolic requirements.[23] An insufficient energy supply leads to neuronal damage, cell death, apoptosis and brain atrophy.[24–26]

A consequence of the CTH model is also that during severely elevated CTH, an increase in CBF could, paradoxically, reduce the delivery of oxygen to the tissue as the oxygen extraction in many capillaries would become critically low.[20] Studies have demonstrated higher CTH in patients with carotid steno-occlusive disease and neurodegenerative disease,[22,27,28] however a direct validation relating CTH to impaired oxygen metabolism has not been provided.

In the present study we tested the CTH model by examining the oxygen metabolism and CTH in patients with precerebral large vessel disease and impaired cerebral hemodynamic. We acquired regional brain maps of CTH (rCTH) and CBF (rCBF) using dynamic contrast-enhanced (DCE) MRI technique, and additionally measured the effect on global $CMRO_2$ ($gCMRO_2$) from elevation of CBF by administration of acetazolamide (ACZ). A high CTH, as previously observed in patients with carotid steno-occlusive disease,[27,28] is likely due to these patients also having varying degree of cerebral small vessel disease.[29] We therefore additionally assessed the patients' white matter hyperintensities (WMH) burden and Fazekas score as indicators of cerebral small vessel disease from structural MRI images.[30] Using this setup we could examine: (1) if patients with intact CVR demonstrate an increase in $gCMRO_2$ following ACZ administration, (2) if patients with impaired CVR demonstrate unaffected, or even decreasing, $gCMRO_2$ from ACZ administration, (3) whether a failure to increase $gCMRO_2$ when elevating CBF can be related to abnormally high rCTH or rCBF steal phenomena, (4) if rCTH correlates with the WMH burden or Fazekas score and if rCTH is higher in WMH compared to normal-appearing white matter (NAWM).

A correlation between CTH and inhibited oxygen metabolism could be a reason why normalizing CBF does not necessarily improve the cerebral oxygen metabolism in patients with steno-occlusive disease. A high CTH could be a pathophysiologically contributing factor leading to declining brain health and atrophy as often observed in this patient group.

Methods

Thirty-four patients with ischemic stroke or transient ischemic attack (TIA) and relevant stenosis or occlusion of the pre-cerebral arteries (common carotid artery (CCA), internal carotid artery (ICA), middle cerebral artery (MCA) or vertebral artery (VA)) were included (17 females, mean age: 68.6 years, age range: 37.2–89.4 years). The patients were recruited from the stroke unit at the Department of Neurology, Rigshospitalet, after a standard protocolled stroke work-up, including neurological examination, acute CT or MRI scan, 48 hours telemetry or Holter, and assessment of the pre-cerebral and cerebral artery stenosis grade by carotid ultrasound imaging and CT angiography. The grading of stenosis or occlusion were based on Doppler velocity criteria.[31] The degree of atherosclerosis was graded by a visual plaque score from 0 to 3, with 2 and 3 being moderate and severe atherosclerosis, respectively.[32]

The CVR status of the patients were evaluated using Single-Photon Emission Computed Tomography (SPECT) imaging or arterial spin labelling (ASL) MRI technique. All patients gave informed consent prior to participation. Patients without the cognitive abilities to give consent and patients with other known brain diseases or short (months) life expectancies were not included in the study. Descriptions of each patient is provided in Table 1. Thirty-one young healthy controls were additionally examined

Table 1. Summary of patients included in the study.

Pt. #	Gender	Age	Grading of pre-cerebral artery stenosis or occlusion		Cerebrovascular reserve capacity impairments	WMH burden [%]	Fazekas score	
			Occlusion	Stenosis			Periventricular WM	Deep WM
1	M	78	Right ICA		Intact	6.62	3	2
2	F	68	Right ICA, left VA		Right hemisphere	1.36	3	3
3	F	55	Right MCA		Bilateral parietal lope	3.05	3	3
4	M	70	Left ICA	Right ICA, right VA	Intact	0.84	1	1
5	M	69	Right CCA		Right hemisphere	0.80	1	1
6	F	71		Bilateral ICA	Right frontal and temporal lope	1.40	1	1
7[a]	F	64	Left MCA		Left parietal lope and frontal lope	17.3	1	2
8	F	73	Left CCA	Right CCA	Left parietal lope Steal phenomenon	3.63	1	2
9	F	65	Left ICA		Intact	3.60	3	2
10	M	65		Bilateral ICA	Intact	0.25	1	1
11	M	72	Left ICA		Left hemisphere. Steal phenomenon.	5.03	2	2
12	F	37	Normal blood flow, moderate atherosclerosis		Intact	0.70	1	1
13	M	67		Bilateral ICA	Intact	7.46	3	2
14	F	62		Right ICA	Right hemisphere	2.46	1	1
15	M	77	Left ICA	Right ICA	Left hemisphere	6.77	2	1
16	F	74	Right ICA	Left ICA	Intact	0.66	1	1
17[a]	F	76		Bilateral ICA	Intact	6.18	2	2
18	F	66	Normal blood flow, moderate atherosclerosis		Intact	0.59	1	1
19[b]	M	70		Right ICA	Intact	3.98	2	2
20	F	89		Bilateral ICA	Intact	6.67	2	1
21	F	68		Bilateral ICA	Intact	2.11	1	1
22[a]	M	78	Normal blood flow, severe atherosclerosis		Intact	3.92	2	2
23	F	60	Normal blood flow, moderate atherosclerosis		Intact	0.03	0	0
24	M	56	Normal blood flow, moderate atherosclerosis		Intact	3.70	2	1
25	M	57	Right ICA	Left ICA	Left frontal and parietal lope	7.83	1	1
26	F	87	Normal blood flow, moderate atherosclerosis		Intact	5.13	2	2
27	M	62	Left ICA	Right ICA	Left hemisphere	4.15	1	1
28	F	64	Normal blood flow, moderate atherosclerosis		Intact	0.70	1	1
29	M	79		Bilateral ICA	Intact	3.46	2	1
30	M	52	Right CCA		Right parietal lope and frontal lope	8.51	1	1
31[b]	M	75		Bilateral ICA	Right hemisphere Steal phenomenon	13.9	1	1
32[b]	M	79		Right ICA	Intact	17.98	3	3
33	M	75	Right ICA	Left ICA	Right hemisphere Steal phenomenon	5.93	1	1
34	F	71	Right ICA	Left ICA, bilateral VA	Right hemisphere Steal phenomenon	3.01	1	1

In total 34 patients participated in the study. Patients had stroke or transient ischemic attack and were included due to symptoms related to pre-cerebral artery steno-occlusive disease. Possible pre-cerebral artery occlusion or stenosis were examined by carotid ultrasound imaging as part of the clinical evaluation before participating in the study. Cerebrovascular reserve capacity (CVR) was evaluated by SPECT imaging or arterial spin labelling MRI technique. In total, 15 patients had reduced CVR and 19 had intact CVR. CCA: common carotid artery; ICA: internal carotid artery; MCA: middle cerebral artery; VA: vertebral artery; WM: white matter; WMH: white matter hyperintensities.

[a]For these three patients, measurements of $gCMRO_2$ were omitted due to technical difficulties or insufficient data quality.

[b]For these three patients, dynamic contrast enhanced (DCE) MRI were not acquired as administration of the MRI contrast agent was not possible.

(13 females, mean age: 23.5 years, age range: 18.1–30.4 years). The study was approved by the Capital Region of Denmark's Committee on Health Research Ethics (H-15003926) and conducted in accordance with the Declaration of Helsinki. The experiment setup is summarised in Figure 1.

MRI protocol

To assess CTH and the effect of ACZ administration on $gCMRO_2$ the participants underwent an MRI-scan. The MRI scans were performed on a Philips 3T Achieva MRI scanner (Philips Medical Systems, Best, The Netherlands) using a 32-channel phased array head coil. From the MRI-scan, measurements of gCBF, $gA\text{-}V.O_2$, and $gCMRO_2$ were obtained using phase contrast-mapping (PCM) and susceptibility-based oximetry (SBO) MRI techniques.[33–35] Baseline measurements were initially acquired, whereafter the participants received an ACZ injection while lying in the MRI-scanner and measurements of gCBF, $gA\text{-}V.O_2$ and $gCMRO_2$ were hereafter repeated. The MRI measurements after ACZ administration were initiated approximately 20 minutes after end of injection. At the end of the MRI scan, approximately 35 minutes after ACZ administration, DCE MRI was used to acquire regional maps of rCBF, rCTH, mean transit times (rMTT) and cerebral blood volume (rCBV). Structural images were acquired in addition to the physiology measurements.

In a subset of the patients ($n = 7$) the CVR status was evaluated using MRI ASL technique. From the ASL sequence rCBF maps were acquired before and after administration of ACZ in the MRI-session.

The scanner was updated approximately halfway through the project to a dSTREAM architecture, which slightly altered some of the sequence parameters in the MRI protocol. The changes are noted in the description of each MRI sequence.

The timing of the MRI-scan is shown in Figure 1.

Global cerebral blood flow

Using PCM MRI the blood velocity and cross-sectional areas of the feeding cerebral arteries (carotids and basilar arteries) were obtained from which gCBF could be calculated. Blood velocity weighted phase-contrast maps were acquired using a turbo field echo sequence (10 repeated measures, 1 imaging plane, field of view (FOV) $= 240 \times 240\,mm^2$, slice thickness $= 8$ mm, voxel size $= 0.75 \times 0.75 \times 8\,mm^3$, echo time (TE) $=$ 7.5 ms, repetition time (TR) $= 12.4$ ms, flip angle $= 10°$, non-gated, velocity encoding (VENC) $= 100$ cm/s).[33,34] Two measurements were acquired. The first measurement with an imaging plane placed orthogonal to the

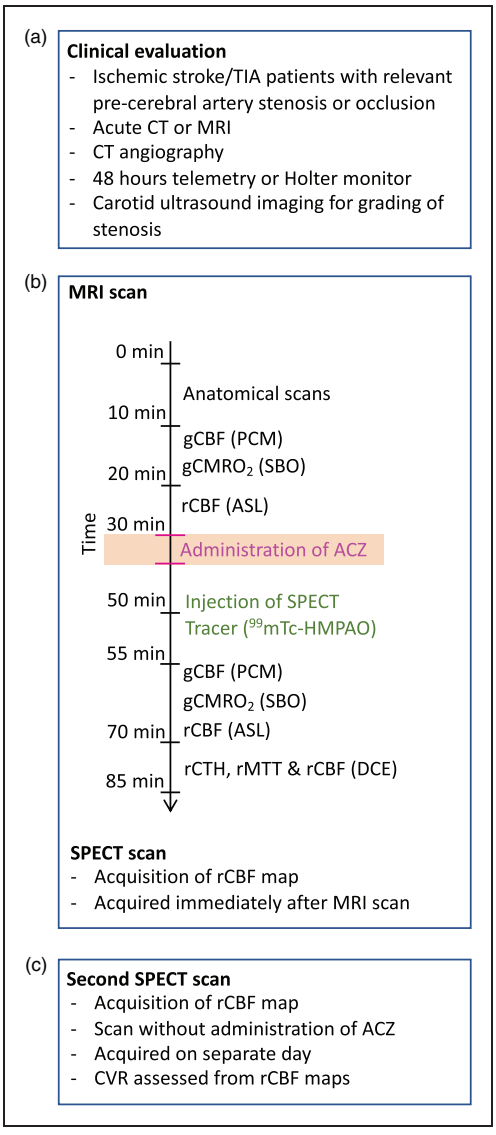

Figure 1. Experiment setup. (a) Patient were recruited based on a clinical evolution when visiting the hospital due to neurological symptoms. Grade of pre-cerebral carotid artery stenosis/occlusion were assessed by ultrasound imaging and/or CT angiography. (b) The participants were MRI scanned from which global cerebral blood flow (gCBF) and metabolic rate of oxygen ($gCMRO_2$) metrics at rest and after administration of ACZ were acquired using phase contrast mapping (PCM) and susceptibility-based oximetry (SBO) MRI sequences. In a subset of the patients ($n = 7$), the cerebrovascular reserve capacity (CVR) status was evaluated by measuring rCBF maps using an arterial spin labelling (ASL) MRI sequence acquired before and after administration of ACZ. Brain maps of capillary transit time heterogeneity (rCTH), cerebral blood flow (rCBF), mean transit times (rMTT) and cerebral blood volume (rCBV) were obtained in the end of the MRI-session using dynamic contrast-enhanced (DCE) MRI technique. The patients were single-photon emission computed tomography (SPECT) scanned immediately after the MRI-scan for assessment of cerebrovascular reserve capacity (CVR) and (c) The patients underwent a second SPECT scan without prior administration of ACZ on a separate day to measure resting perfusion maps as part of the calculated of CVR.

carotid arteries and the second measurement with an imaging slice placed orthogonal to the basilar artery. This ensured that the imaging planes could be placed correctly orthogonal on the respective arteries to minimize partial volume contamination in the measurements.[36,37] The blood flows in the cerebral feeding arteries were calculated by multiplying the mean blood velocity by the cross-sectional area from regions of interest (ROIs) defining each vessel. The global mean CBF was calculated by normalizing the total cerebral blood flow to the brain weight. Brain weight was calculated from the structural MRI images and assuming a brain density of 1.05 g/ml.[38]

Cerebral metabolic rate of oxygen

Using the SBO MRI technique the venous oxygen saturation (S_vO_2) of the blood leaving the brain was measured.[35] The technique utilizes that the magnetic susceptibility of the blood can be related to the deoxyhemoglobin concentration. With additional measurements of arterial oxygen saturation (S_aO_2) from pulse oximetry, gA-V.O_2 could be calculated by subtracting S_vO_2 from S_aO_2 (equation (1)).

$$\text{gA-V.O}_2 = S_aO_2 - S_vO_2 \quad (1)$$

Using the Fick's principle, $gCMRO_2$ could then be calculated by equation (2).

$$gCMRO_2 = [\text{Hgb}] \cdot \text{gCBF} \cdot \text{gA-V.O}_2 \quad (2)$$

The hemoglobin concentration (Hgb) was assumed 9.1 mmol/l for all subjects. The imaging plane for the SBO sequence was placed orthogonal to the sagittal sinus to measure on the blood immediately leaving the brain. Magnetic susceptibility-weighted maps were generated by a dual–echo gradient echo sequence (20 repeated measures, 1 imaging plane, FOV = 224 × 176 mm^2, voxel size = 0.5 × 0.5 × 8 mm^3, TR = 27.5 ms, TE1 = 7.0 ms, TE2 = 20.3 ms, flip angle = 30°, before the scanner update and adjusted to FOV = 220 × 180 mm^2, voxel size = 0.69 × 0.69 × 8 mm^3, TR = 23.1 ms, TE1 = 8.0 ms, TE2 = 17.7 ms, Flip angle = 30°, SENSE factor = 2 after the scanner update). By subtracting phase value maps from the two echoes, susceptibility-weighted maps were calculated. Aliased phase values in the sagittal sinus and the immediately surrounding tissue were manually corrected. By use of intravascular susceptibility values from the sagittal sinus and susceptibility values from the immediately surrounding brain tissue the oxygen saturation can be calculated.[35] An in-depth discussion of the sequence and postprocessing has been provided previously.[39] The technique has been validated against oxygen saturation measurements from blood samples acquired by catheter from the jugular vein during MRI-scanning.[40] The technique was validated at rest and during hyperperfused conditions.[40]

Regional cerebral blood flow and capillary transit time heterogeneity

Brain maps of rCTH were obtained using the DCE MRI technique.[28,41] The method utilizes that the presence of MRI contrast agent (CA) in the blood changes the T_1 relaxation of the acquired MRI-signal. By acquiring dynamic measurement of T_1-weigthed images during the CA bolus passage through the brain, CBF and transit times can be calculated using kinetic modelling. A 2D saturation recovery gradient recalled sequence was used both for an initial T_1 measurement and for the subsequent dynamic imaging (300–500 repeated measures, 5 slices, time resolution = 1.25 s, FOV = 230 × 182 × 40 mm^3, acquired voxel size = 2.4 × 3.0 × 8 mm^3, reconstructed voxel size = 0.9 × 0.9 × 8 mm^3, TR = 3.95 ms, TE = 1.92 ms, flip angle = 30°, centric phase ordering, SENSE factor = 2 before the scanner update and adjusted to 350 repeated measures, time resolution = 1.25 s, TE = 1.97 ms after the scanner update). The T_1 weighted images were acquired after application of a non-selective saturation pre-pulse with a saturation time delay (TD). The initial T_1 measurement was performed by varying the TD value (120 ms, 300 ms, 600 ms, 1 s, 2 s, 4 s, 10 s). The dynamic measurements of the CA bolus passage were acquired using a fixed TD of 120 ms. The most caudal slice was, independently of the other slices, placed orthogonally to the internal carotid artery (ICA) based on an MRI angiogram in order to obtain an arterial input function (*AIF*) of the CA concentration immediately before entering the brain. The remaining four slices were placed with the corpus collosum approximately being the center of the acquisition. The gadolinium based Gadovist (Bayer HealthCare Pharmaceuticals, Berlin, Germany) was used as CA in a solution of 1.0 mmol/ml. Two boluses of CA were administrated with initiations at measurement number 15 and 70 of the dynamic imaging.[28] For each bolus the dose CA was 0.045 mmol/kg injected with 3 ml/s followed by 20 ml saline using an automatic CA injector (Medrad Spectris Solaris MR injector system, Pennsylvania, USA). The MR signal during the bolus passage was converted to CA concentration as a single point resolved T_1 determination using the initial T_1 measurement and assuming a fast water exchange regime.[24] All tracer kinetic modeling was done in the concentration domain. The CA concentration (C_t) in the acquired

MRI-images was modelled in each voxel as the convolution between the *AIF* and the residue impulse function (*RIF*) of the tissue scaled by blood flow (*F*) as demonstrated in equation (3).

$$C_t(t) = AIF(t) \otimes \mathrm{F}\ RIF(\mathrm{t}) = F\int_0^t AIF(\tau)RIF(t-\tau)\mathrm{d}\tau \quad (3)$$

The pixels in the center of the ICA were used to measure the *AIF*. The *AIF* was further scaled with a venous outflow curve obtained from the sagittal sinus in order to reduce the partial volume effect. The *AIF* was time shifted to local tissue curves to ensure synchronicity. This was achieved pixelwise by taking an initial short segment of the *AIF* and tissue curve and applying a simple deconvolution using a monoexponential residue impulse as kernel, from which the time offset could be acquired.

The distribution of transit times (*h*), also called the frequency function, was defined as the fraction of CA leaving the tissue as a function of time, which can be related to *RIF* as demonstrated in equation (4).

$$RIF(t) = 1 - \int_0^t h(\tau)\mathrm{d}\tau \quad (4)$$

A gamma function distribution was used to describe *h*, corresponding to the classical distribution of frequency function of transit times.[42] CTH was then calculated as the standard deviation of *h* (equation (5)).

$$CTH = \mathrm{std}(h(t)) \quad (5)$$

MTT was calculated as the integral of RIF(t) (equation (6)).

$$MTT = \int_0^\infty RIF(t)\mathrm{d}t \quad (6)$$

Blood flow and blood volume was modelled separately by use of Tikhonov's generalized singular value decomposition as previously described.[41] Thus, the kinetic modelling resulted in the calculation of parameters maps describing rCBF, rCBV, rMTT and rCTH.

The ratio between rCTH and rMTT (rCTH/rMTT), often called the *relative transit-time heterogeneity,* was additionally calculated. In a normal healthy cerebral microvascular network, CTH will be affected in parallel with changes of MTT.[43] For example a reduction in MTT from increased CBF would also reduce CTH. However, in tissue with capillary flow disturbances CTH will likely not change with a same degree as MTT, which will result in a high rCTH to rMTT ratio. The rCTH to rMTT ratio could therefore be a better descriptor of microvascular distribution disturbances than CTH alone, as the ratio considers a possible effect from differences in MTT.[43]

In-depth description of the method and calculation of CTH has been published previously.[28]

The calculated parameter maps were co-registered to the individual anatomical images using image header information. The anatomical maps were co-registered to standard MNI space by first applying a linear affine transformation and hereafter non-linearly warping using the FSL software package.[44] The linear and non-linear transformations of the anatomical images to MNI space were then applied to the parameter maps. Mean values from ROIs defining the vascular territories for the middle carotid arteries (MCA), anterior carotid arteries (ACA) and posterior carotid arteries (PCA) were extracted from the parameter maps.[45,46] In patient with impaired CVR, values were extracted from the affected areas corresponding to the vascular territories. Values from the contralateral regions were extracted as measurement of CVR in intact regions. If the whole hemisphere were affected the average values from all ROIs in the hemisphere were used in the further analysis. For patients with intact CVR, and in the control subjects, the average values of all the vascular territory ROIs were acquired and used in the further analysis.

Examples of rCTH, rCBF, rMTT and rCBV maps calculated from the DCE analyses with indication of the vascular territory ROIs are shown in Figure 2.

Anatomical imaging and white matter hyperintensities

High-resolution anatomical images were measured with a 3D *T1*-weigthed turbo field echo sequence (150 slices, FOV = $241 \times 180 \times 165\,\mathrm{mm}^3$, voxel size = $1.09 \times 0.81 \times 1.1\,\mathrm{mm}^3$, TR = 6.9 ms, TE = 2.78 ms, flip angle = 9° before scanner update and adjusted to 257 slices, FOV = $256 \times 256 \times 180\,\mathrm{mm}^3$, voxel size = $0.67 \times 0.67 \times 0.7\,\mathrm{mm}^3$, TR = 11.3 ms, TE = 5.7 ms, flip angle = 8° degrees after scanner update). The images were segmented for grey matter, white matter, and cerebrospinal fluid (CSF) using the FSL-functions BET and FAST (FMRIB Software Library, Oxford University).[44] A brain mask covering the cerebrum, cerebellum, and brainstem was created to obtain the total brain volume.

A fluid attenuated inversion recovery (FLAIR) sequence were used to acquire brain

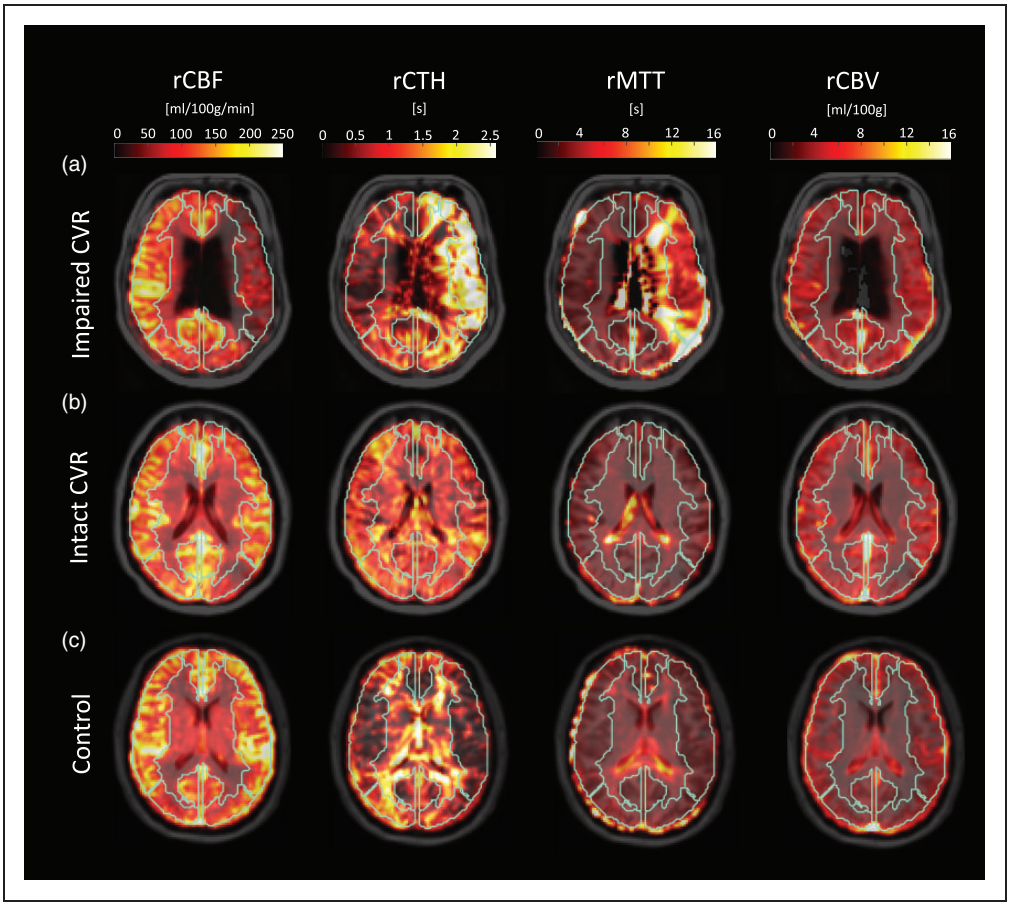

Figure 2. Example of parameter maps acquired by dynamic contrast-enhanced (DCE) MRI. Examples of brain maps demonstrating cerebral blood flow (rCBF), capillary transit time heterogeneity (rCTH), mean transit time (rMTT) and cerebral blood volume (rCBV) in a patient with impaired cerebrovascular reserve capacity (CVR) (A), a patient with intact CVR (B) and a healthy control subject (C) are shown. The data were measured approximately 35 minutes after administration of acetazolamide (ACZ). The regions of interests approximately defining the vascular territories of middle carotid artery (MCA), anterior carotid artery (ACA) and posterior carotid artery (PCA) are demonstrated by the blue lines. In the patient with impaired CVR a reduced rCBF, elevated rCTH and high rMTT in the affected brain hemisphere are clearly visible.

images for assessment of the WMH burden of the patients (31 slices, FOV = $230 \times 154 \times 183\,mm^3$, voxel size = $0.45 \times 0.45 \times 4\,mm^3$, TR = 11000 ms, TE = 125 ms, flip angle = 90°, inversion time (TI) = 2800 ms before scanner update and adjusted to 28 slices, FOV = $230 \times 139 \times 182\,mm^3$, voxel size = $0.60 \times 0.60 \times 4\,mm^3$, TR = 11000 ms, TE = 125 ms, flip angle = 90° degrees after scanner update). A white matter hyperintensities (WMH) mask were created by manual delineation using the FLAIR images. The global WMH burden were calculated as the ratio between WMH volume and total white matter volume. A Fazekas score was additionally obtained for the participants.[30] The combined Fazekas score of periventricular white matter hyperintensities and deep white matter hyperintensities was used resulting in a grading from 0 to 6. Global WMH burden and Fazekas score from each patient is noted in Table 1.

Cerebrovascular reserve capacity

As part of the clinical evaluations the patients underwent examination of CVR by SPECT scanning using technetium-99m hexamethylpropyleneamine oxime (^{99}mTc-HMPAO) as tracer. From the SPECT data rCBF maps could be calculated in a semi-quantitative manner (EXINI brain; EXINI diagnostics AB, Lund, Sweden).[47,48] Two SPECTS scans were obtained. The first SPECT scan was acquired immediately after the MRI scan. The ^{99}mTc-HMPAO-tracer was administered, while the subject was lying in the MRI-scanner, approximately 20 minutes after administration of ACZ. The ACZ dose were determined based on the participant weight (<40 kg = 0.5 g, 40–50 kg = 0.75 g, 50–65 kg = 1.0 g, 65–80 = 1.25 g, >80 kg = 1.5 g) and injected into a superficial cubital vein in a saline solution over

a period of 5 minutes. A second SPECT scan without administration of ACZ was performed on a subsequent day. From the resting rCBF data acquired without ACZ and the measurement after elevation of rCBF from administration of ACZ, CVR maps could be calculated using EXINI brain software.[47,48] A minority of patients (n = 7) did not undergo SPECT scanning, instead the ASL imaging from the MRI scans were used to calculate rCBF maps from which the CVR status could be determined. The ASL CBF maps were measured using a 2D sequence with a pseudo-continuous arterial spin labelling scheme (pcASL) and image acquisition at seven different TI (12 slices; FOV = $220 \times 220 \times 78\,mm^3$, voxel size = $3.4 \times 3.4 \times 6\,mm^3$, TR = 300 ms, TE = 10.79 ms, flip angle = 40°, labelling duration = 1650 ms, TIs = 100 ms, 400 ms, 700 ms, 1000 ms, 1300 ms, 1600 ms and 1900 ms). The ASL sequence was acquired at baseline and after administration of ACZ. The ASL data was analysed using the function *Oxford ASL* as part of the FSL software package (FMRIB Software Library, Functional Magnetic Resonance Imaging of the Brain Centre, Department of Clinical Neurology, University of Oxford, Oxford, UK).[44,49]

Classification of CVR was evaluated by experienced medical doctors as part of the clinical evaluation of the patients. Patients were classified into normal CVR or impaired CVR groups and the affected brain regions were found (Table 1). Some patients demonstrated a CBF steal phenomenon, where ACZ administration causes a focal decrease in CBF in the vascular territories supplied by a stenotic or occluded artery. This phenomenon is a result of the vessel in the affected region already being maximal dilated and a reduction in perfusion pressure in the remaining more normally perfused regions of brain following ACZ administration.[50–52] A steal phenomenon from ACZ administration could potentially affect the oxygen metabolism if the perfusion in these regions become critically low. The presence of CBF steal phenomena is noted in Table 1.

Statistics

The postprocessing of the MRI-data was blinded to the subject's group (patient or control) and measurement (baseline measurement or measurement after ACZ administration). Generally, values are noted as mean ± standard deviation throughout the paper. P-values less than 0.05 were considered significant. Normal distribution of the parameters was confirmed with the Shapiro-Wilk normality test before entering the statistical models when necessary.

The effect from ACZ administration on gCBF, gA-V.O_2 and $gCMRO_2$ were tested using paired Students' t-test (Figure 3). Differences in baseline gCBF, gA-V.O_2 and $gCMRO_2$ between the patients and controls were assessed by unpaired Students' t-tests (Figure 3). Correlations between changes in gCBF and $gCMRO_2$ from administration of ACZ were examined by linear mixed model with $gCMRO_2$ as response variable, gCBF as the fixed effect and subject identification as random effect (Figure 4). Differences in rCBF, rCTH, rMTT, rCTH/rMTT and rCBV between CVR-impaired regions and CVR-intact regions were tested using paired Students' t-tests (Figure 5a–e). Differences in rCTH, rCBF, rMTT, rCTH/rMTT and rCBV between patients and controls were tested using unpaired Students' t-tests (Figure 5a–e). To test whether a possible reduction in $gCMRO_2$ from ACZ administration ($\Delta_{ACZ.}gCMRO_2$) could be correlated to high CTH or low CBF (possible from CBF steal phenomenon) a linear regression model with rCTH and rCBF as regressors and $\Delta_{ACZ.}gCMRO_2$ as dependent variable were used (equation (7)).

$$\Delta_{ACZ.}gCMRO_2 = \beta_1 \cdot rCTH + \beta_2 \cdot rCBF \qquad (7)$$

Two models were calculated: A model with rCTH and rCBF values from CVR-intact regions and a model with rCTH and rCBF values from CVR-impaired regions. Partial regression plot demonstrating the correlations between $\Delta_{ACZ.}gCMRO_2$ and rCTH or rCBF are shown in Figure 6. We additionally calculated a model with rCTH/rMTT instead of rCTH as the regressor, which similarly is demonstrated in Figure 6. We further tested whether the model including both rCTH and rCBF as regressors performed significantly better than a model with only rCBF as a single regressor using F-test statistics of the models.

Lastly, we examined for correlations between rCTH and white matter alterations by correlating WMH burden and Fazekas score to white matter rCTH using linear regression models. We further tested for differences in rCTH and rCBF in regions classified as WMH compared to NAWM using paired Students' t-tests and for differences in white matter rCTH and rCBF in patients compared to the control group using unpaired Student's t-tests (Figure 5f and g).

Results

Attrition and missing data

In one patient measurement of $gCMRO_2$ failed due to ghosting artefacts on the MRI images. In two more patients, measurement of $gCMRO_2$ were omitted due to technical difficulties at the time of the MRI-scan making the technique unavailable. Two healthy controls subjects had a bifurcation of the sagittal sinus

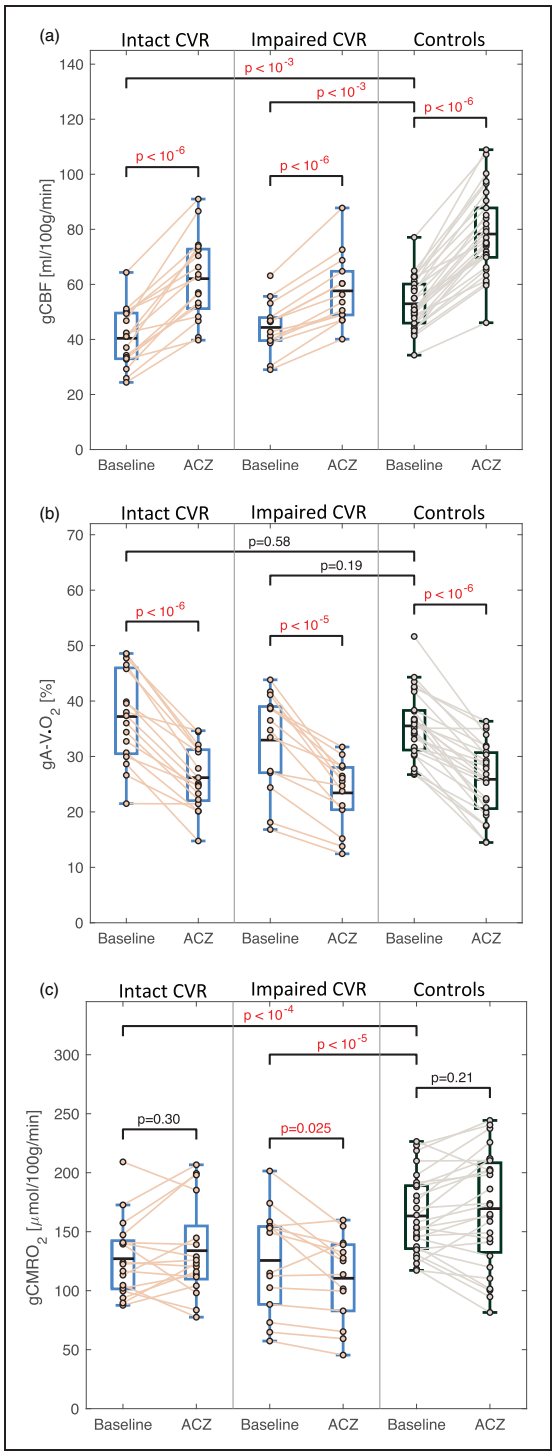

Figure 3. Boxplots demonstrating (a) global cerebral blood flow (gCBF), (b) arteriovenous oxygen extraction (gA-V.O_2) and (c) cerebral metabolic rate of oxygen (gCMRO_2) at baseline and after acetazolamide (ACZ) administration. Each panel demonstrate values for patients with intact cerebrovascular reserve capacity (CVR) (a), for patients with impaired CVR (b) and for healthy control subjects (c). Administration of ACZ significantly increased gCBF and reduced gA-V.O_2 as expected. Patients with impaired CVR had a significant reduction in gCMRO_2 after administration of ACZ.

making the measurement of S_vO_2 and thereby calculation of gCMRO_2 unreliable.[53] These measurements were removed from the further analysis. For three patients DCE-MRI were not acquired as administration of the MRI contrast agent were not possible for these patients.

Cerebrovascular reserve capacity

Out of the 34 patients who participated in the study, 15 (44%) had impaired CVR and the remaining 19 (56%) patients had intact CVR (Table 1). Five of the patients with impaired CVR demonstrated a steal phenomenon in the affected hemisphere. Two of these patients only demonstrated a minor steal phenomenon (~5% reduction in CBF) and the remaining a more pronounced effect.

Cerebral blood flow and oxygen metabolism

Boxplots of gCBF, gA-V.O_2 and gCMRO_2 at baseline and after administration of ACZ for each group are shown in Figure 3. Administration of ACZ increased gCBF and reduced gA-V.O_2 in all groups ($p < 10^{-5}$), as expected. gCMRO_2 was significantly reduced in the patient group with impaired CVR ($p = 0.025$) but unaffected in the other groups. The correlations between change in gCBF and gCMRO_2 from ACZ administration are demonstrated in Figure 4. We observed a significant positive correlation demonstrating increase in gCMRO_2 with increasing CBF in the patient group with intact CVR ($\beta = 0.59 \frac{\mu\text{mol } O_2}{\text{ml blood}}$, $p = 0.018$). There were no correlations in the group with impaired CVR ($p = 0.085$) or the control group ($p = 0.091$). Overall, these results demonstrate that in the patients with intact CVR the oxygen metabolism is increased by elevating CBF.

Capillary transit time heterogeneity

Possible causes for a reduced gCMRO_2 after ACZ administration could be a high CTH impairing oxygen extraction or presence of CBF-steal phenomenon critically reducing the perfusion. We examined these possibilities by acquiring regional maps of rCTH and rCBF after administration of ACZ (examples of calculated maps are shown in Figure 2). Boxplots of rCBF, rCTH, rMTT, rCTH/rMTT and rCBV in CVR-impaired regions, CVR-intact regions and in healthy controls are shown in Figure 5(a–e). CVR-impaired regions had significantly reduced rCBF compared to CVR-intact regions ($p < 10^{-4}$) and controls ($p < 10^{-4}$), as expected. rCTH and rMTT were significantly higher in CVR-impaired regions compared to CVR-intact regions ($p = 0.022$ for rCTH and $p = 0.002$ for rMTT) and compared to controls

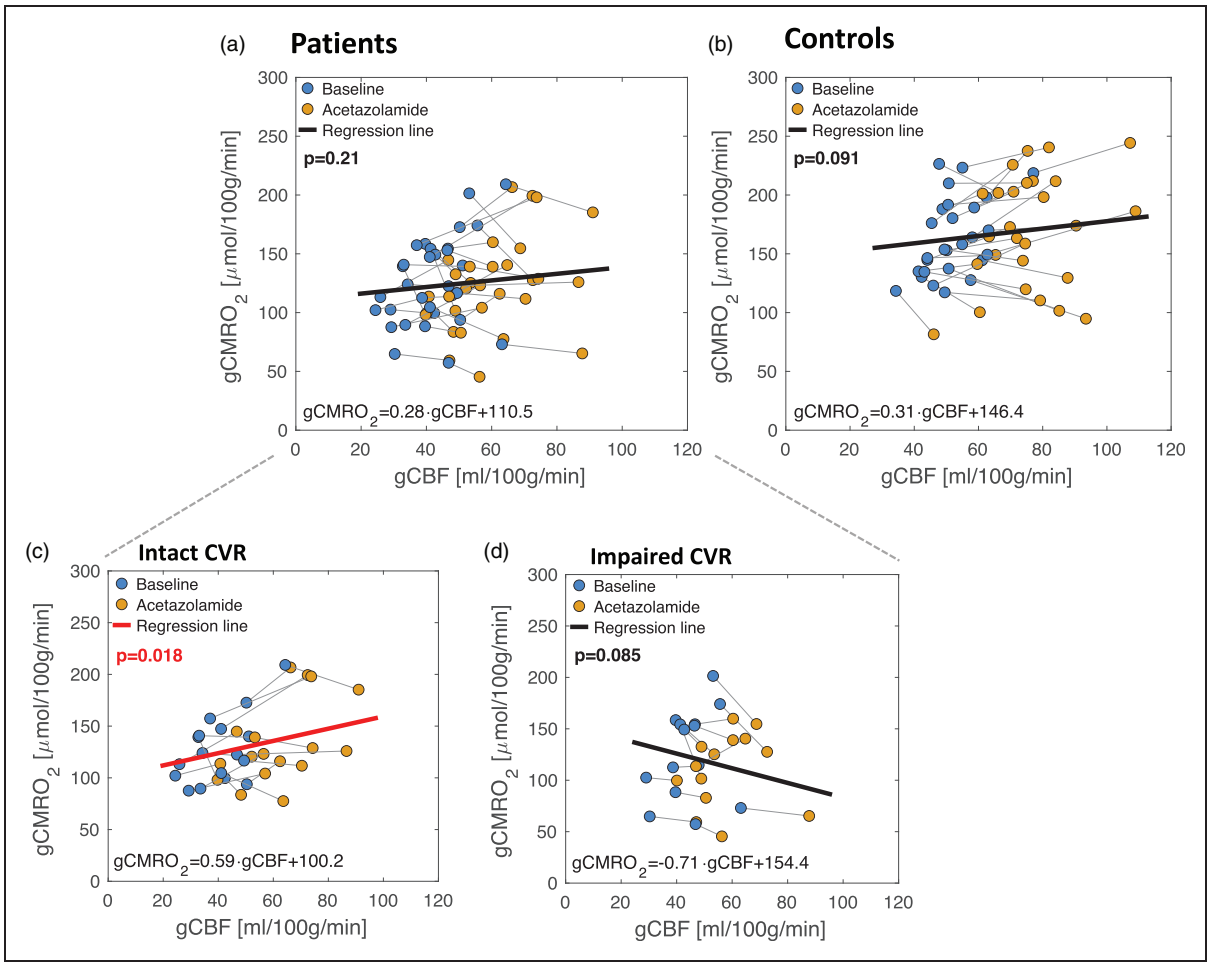

Figure 4. Correlations between global cerebral blood flow (gCBF) and global cerebral metabolic rate of oxygen ($gCMRO_2$) at resting and after administration of acetazolamide (ACZ) in patients and healthy controls. (a) Overall, patients with carotid steno-occlusive disease demonstrated no correlation between change in gCBF and change in $gCMRO_2$ from ACZ administration. (b) Similarly, the $gCMRO_2$ was unaffected from elevated CBF in control subjects. (c) If the patients were split into CVR-impaired and CVR-intact patients a significant positive correlation is observed between change in $gCMRO_2$ and gCBF in the patients with intact CVR and (d) In the group with impaired CVR there was a tendency for a decreased in $gCMRO_2$ for increasing gCBF, however the correlation was not significant.

($p = 0.005$ for rCTH and $p < 10^{-6}$ for rMTT). rCTH/rMTT was not significantly different between CVR-impaired regions compared to CVR-intact regions ($p = 0.64$) or healthy controls ($p = 0.27$). rCBV was significantly higher in patients compared to control subjects ($p < 10^{-4}$), but no differences were observed between CVR-intact and CVR-impaired regions ($p = 0.12$). Overall, these results demonstrate that in CVR-impaired regions, in addition to a reduced perfusion, the capillary transit times are abnormally distributed demonstrated by higher CTH.

We hereafter examined whether the abnormal rCBF or rCTH could explain the change in $gCMRO_2$ from ACZ administration ($\Delta_{ACZ}gCMRO_2$) by linear regression models with both rCBF and rCTH as regressors. Partial regression plots demonstrating the correlations from the models are shown in Figure 6. We observed a significant negative correlation ($p = 0.023$) between $\Delta_{ACZ}gCMRO_2$ and rCTH in CVR-impaired regions, but no correlation for rCTH in CVR-intact regions. Similarly, low rCBF in CVR-impaired regions correlated with decreasing $\Delta_{ACZ}gCMRO_2$ ($p = 0.008$). We hereafter tested whether the model including both rCTH and rCBF as regressors were significantly better than a model with only rCBF as regressor using F-test statistics. We observed a significant ($p = 0.026$) better model when rCTH were included, further substantiating the observation that high rCTH contributes to an impaired oxygen metabolism. Lastly, we examined a model with rCTH/rMTT instead of rCTH and similarly found a significant correlation between high rCTH/rMTT in CVR-impaired regions

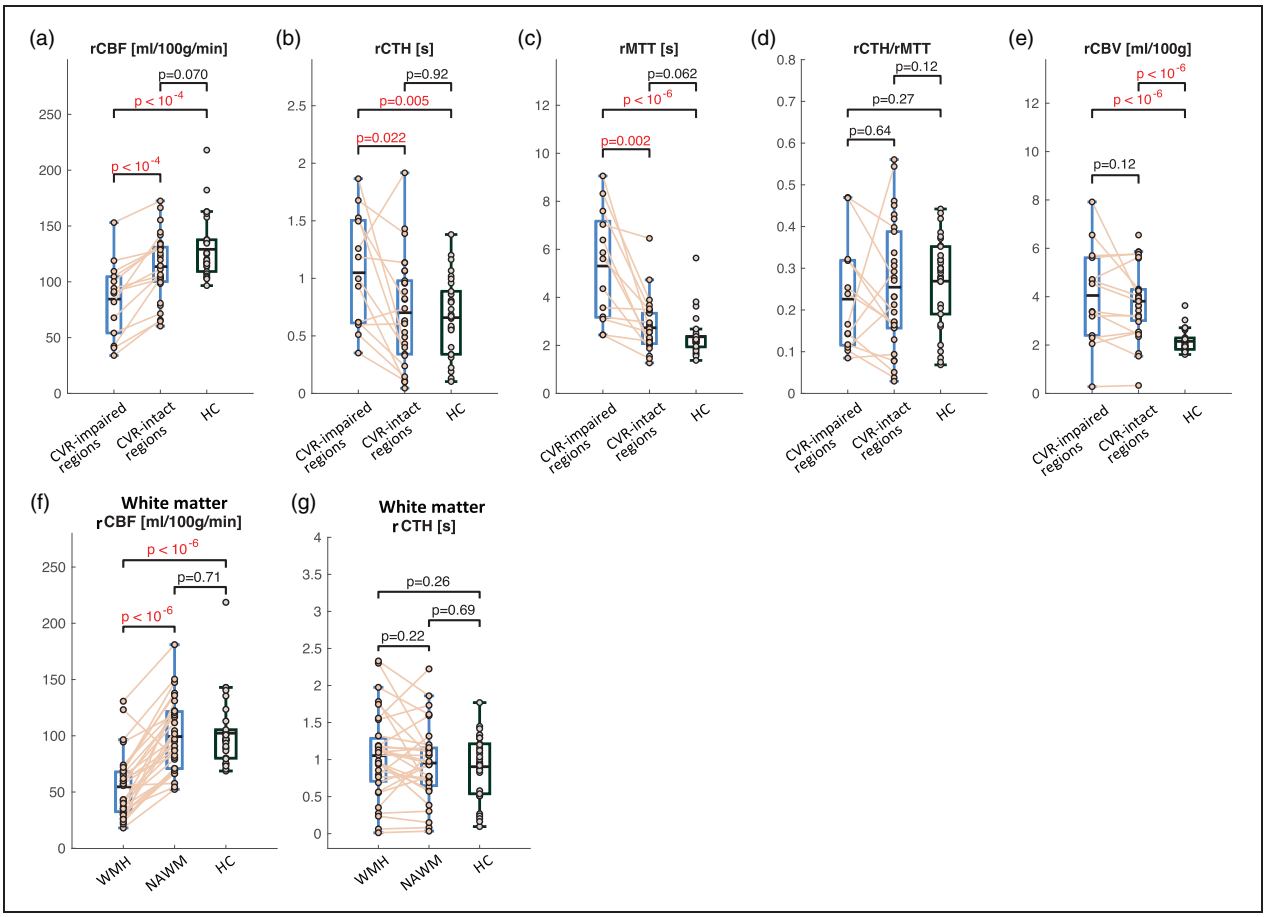

Figure 5. Boxplot of regional cerebral blood flow (rCBF), capillary transit time heterogeneity (rCTH), mean transit time (rMTT), rCTH to rMTT ratio (rCTH/rMTT) and cerebral blood volume (rCBV). The parameters were acquired using dynamic contrast-enhanced (DCE) MRI. (a) rCBF was significantly reduced in regions with impaired cerebrovascular reserve capacity (CVR) compared to CVR-intact regions and healthy controls (HC), as expected. Both rCTH (b) and rMTT (c) were significantly higher in CVR-impaired regions compared to CVR-intact regions and compared to HC. (d) rCTH/rMTT was not significantly different between CVR impaired and CVR intact regions or healthy controls. (e) rCBV were significantly higher in patients (both CVR-impaired and CVR-intact regions) compared to HC. (f) rCTH was not significantly different in white matter hyperintensities (WMH) compared to normal appearing white matter (NAWM) or white matter in HC and (g) rCBF was significantly lower in WMH compared to NAWM and compared to white matter of healthy controls.

and decreasing $\Delta_{ACZ}gCMRO_2$ ($p = 0.017$). There was no correlation between rCTH and $\Delta_{ACZ}gCMRO_2$ in the healthy control group ($p > 0.26$) (not shown). Overall, these results indicate that both high rCTH and low rCBF contributes to an impaired oxygen metabolism.

Lastly, we examined whether the presence of WMH was associated with high rCTH. We did not observe higher CTH in WMH compared to NAWM or white matter of healthy controls (Figure 5(e)) and did not find any correlations with WMH burden ($p = 0.11$) or Fazekas score ($p = 0.83$). CBF were, however, significantly reduced ($p < 10^{-6}$) in WMH compared to NAWM and compared to white matter of healthy controls (Figure 5(f)). These results suggest that the white matter alteration observed in the patients can primarily be related to hypoperfusion and not abnormal CTH.

Discussion

In the present study we observed a paradoxical reduction in $gCMRO_2$ when the cerebral perfusion is elevated by administration of ACZ in some patients with impaired CVR. The reduction in oxygen consumption could be related to high rCTH, high rCTH to MTT ratio and low rCBF in CVR-impaired regions. The correlation between high CTH and reduced $gCMRO_2$ is in line with the CTH theory suggesting that disruption of the microperfusion causing uneven distribution of capillary flow and transit times could limit the cerebral extraction of oxygen.[15] When CBF is elevated by

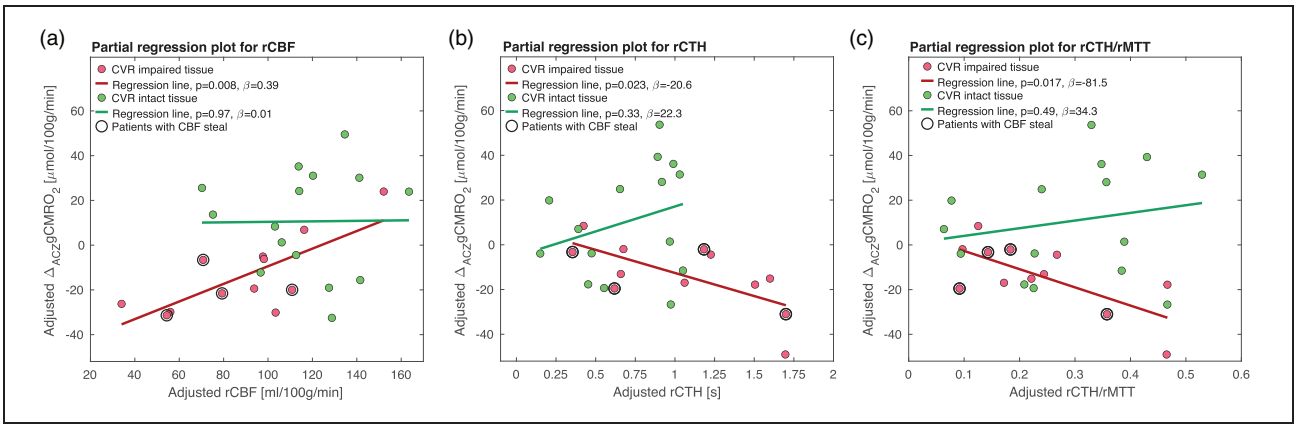

Figure 6. Correlations between (a) cerebral blood flow (rCBF), (b) capillary transit time heterogeneity (rCTH) and (c) rCTH to mean transit time (rMTT) ratio (rCTH/rMTT) and change in cerebral metabolic rate of oxygen ($\Delta_{ACZ}gCMRO_2$) from administration of acetazolamide (ACZ). Brain regions with impaired cerebrovascular reserve capacity (CVR) demonstrate a significant negative correlation between rCTH and $\Delta_{ACZ}gCMRO_2$. In contrast, CTH in CVR-intact regions did not correlate with $\Delta_{ACZ}gCMRO_2$. Similar significant correlations were observed for rCTH/rMTT and $\Delta_{ACZ}gCMRO_2$. Low rCBF in CVR-impaired regions also correlated significantly with decreasing $\Delta_{ACZ}gCMRO_2$. Overall, these results suggests that both low rCBF and high rCTH in CVR-impaired tissue contribute to an inhibit oxygen metabolism.

ACZ administration the uneven distribution may be further aggravated causing a reduction in the oxygen extraction and oxygen consumption, as has been hypothesized based on mathematical models.[15,20] In the CVR-impaired regions, the stenosis or occlusion of the upstream cerebral arteries inhibits perfusion to the affected area. Additionally, small vessel disease in the affected region could further limit the CVR due to reduced or missing vasomotor function in the arterioles and capillaries from endothelial damages.[54,55] Dysfunctions of the small vessels are likely also the cause for the high CTH in these regions. The CVR-impaired tissue is in state of hypoperfusion causing local hypoxia and hypometabolism. This environment will, in addition to harming neurons and glia cells, also damage the vessel endothelia, vascular smooth muscle cells and pericytes. Damages to the endothelium cells and pericytes will hinder the vasomotor skill of the capillaries. Additionally, ischemic damage or necrosis of pericytes can cause a state of permanent pericyte and capillary constriction.[56] Overall, these damages can cause dysfunction of the perfusion modulation in the capillary bed which will cause an uneven distribution of flow and transit times, as demonstrated by the high CTH. The higher CTH we observed in the patients is in line with two prior studies which similarly found higher CTH in patients with steno-occlusive disease[27,57] and that treatment by carotid artery stenting reduces CTH in the affected brain regions.[57] Furthermore, it has been shown based on estimation of the maximal oxygen extraction from the CTH hypothesis, that the oxygen extraction level observed in brain regions affected by carotid occlusion is better explained when taking the elevated CTH into account than just the hypoperfusion alone.[23]

However, these studies did not measure if the patients demonstrate an inhibited oxygen consumption and if elevated flow further reduces the oxygen consumption in accordance with the CTH theory. In present study we demonstrate that the higher CTH seen in CVR-impaired patients indeed has a harmful effect on the cerebral oxygen metabolism. High CTH could therefore be a contributing part to the declining brain health and neurodegeneration observed in patients with cerebral and precerebral large and small vessel disease, as these patients demonstrate both hypoperfusion and impaired oxygen extraction causing detrimental metabolic inadequacies. High CTH could also be a reason why normalizing CBF by endarterectomy or carotid angioplasty in some patients does not improve the oxygen metabolism.

In addition to the effect from rCTH, we also observed a significant positive correlation between rCBF in CVR-impaired regions and change in $gCMRO_2$ after ACZ administration from the regression model (equation (7)). This correlation indicates that having a high rCBF has a beneficial effect on maintaining $CMRO_2$ independent from the rCTH level. On contrast, if the patient has a low rCBF, which might be aggravated from a CBF steal phenomenon, the perfusion is inadequate to maintain $CMRO_2$. The reduction in $CMRO_2$ observed in some patients is therefore a combination of low rCBF and an elevated rCTH.

When examining the white matter of the patients we observed reduced perfusion in WMH compared to

NAWM, but no differences were observed for CTH. These results suggest that inhibition of oxygen metabolism from CTH primarily is affecting grey matter structures and damages to white matter is from inadequate perfusion. Grey matter has a higher metabolism and oxygen extraction compared to white matter,[58] which suggest that an inhibition of the oxygen extraction will affect grey matter more severely. These observations are somewhat in contrast to Dalby et al.[59] who observed higher CTH in WMH compared to NAWM and Kaczmars et al.[27] who observed higher CTH in both white matter and grey matter in patients with asymptomatically carotid stenosis. A possible explanation for the discrepancy could be that the patient examined in our study have more severe hemodynamic deficits with some patients demonstrating full occlusion of the cerebral arteries and consequently hypoperfusion and CVR impairments. The severe hypoperfusion and CVR impairment could dominate the alteration of white matter structures observe in our study.

In contrast to the patients with impaired CVR, in the group with intact CVR we observed a significant increase in $gCMRO_2$ with increasing CBF from ACZ administration. This increase in $gCMRO_2$ suggests that these patients can have a beneficial effect on the cerebral metabolism from elevated CBF if CTH is not pathologically elevated. In these patients the cerebral vessels are not fully dilated at their normal resting condition and there exist and CBF reserve capacity that can be recruited through stimulated vasodilation. However, we still observed that the resting CBF is reduced compared to healthy controls. A potential cause for the hypoperfusion could be due to the initiation of different adaptive processes for the brain to function under less perfusion and oxygen availability.[60–62] A potential mechanism could be to reduce the oxygen demand by apoptosis, which over time becomes an irreversible reduction of brain cells and function.[63,64] Early treatment normalizing CBF could potentially stop these mechanisms and help to maintain oxygen metabolism and avoid severe cell death and atrophy.

Strength and limitation

The main limitation of the study is that we only acquired global values of $gCMRO_2$. Patient with impaired CVR demonstrate asymmetrical regional limitations corresponding to the carotid disease lateralization. The effect on $gCMRO_2$ observed in this group is most likely driven by disruptions in the affected region. This also corresponds that abnormal CTH is only observed in the affected side. By regional measurement of $CMRO_2$ this could be elucidated. New MRI techniques are under development for regional acquisition of quantitative OEF and $gCMRO_2$, however these methods are not yet validated or widely available.[65] Hopefully these methods can be applied in future studies.

Another limitation is that the control group is not age-matched but consists of younger individuals. However, as we do not observe any differences of rCTH in CVR-intact tissue in the patient group compared to controls we do not expect that an older control group would demonstrate different values. An older age matched control group would then not affect the conclusion of the study.

A main strength of the experiment was that we acquired both measurement of rCTH and the $gCMRO_2$ response to elevated CBF in a single MRI scan session. Measurements of oxygen saturation in the sagittal sinus for $CMRO_2$ calculation by SBO MRI technique have been validated against blood samples acquired by catheter from the jugular vein during MRI-scanning.[40] The validation was performed both at rest and during hyperperfused conditions.[40] Global CBF measured using PCM MRI and regional CBF by ASL technique has been validated in animal models and humans against ^{15}O-water PET imaging as accepted gold standard reference.[34,66–69]

Conclusion

In this study we observed reduced oxygen metabolism in response to elevated CBF from ACZ administration in some patients with impaired CVR from steno-occlusive cerebral artery disease. The impaired oxygen metabolism could be related to uneven distribution of capillary microperfusion characterized by CTH and to low perfusion in the affected brain regions. A high CTH could be a contributing factor to the declining brain health and higher risk of neurodegenerative disease observed in patients with carotid stenosis or occlusion. We further observed that patient with intact CVR did not demonstrate abnormal CTH and that these patients had a beneficial effect on the oxygen metabolism from increased perfusion.

Funding

The author(s) disclosed receipt of the following financial support for the research, authorship, and/or publication of this article: Mark B. Vestergaard was supported by grants from The Danish Council for Independent Research (8020-00251B) and Rigshospitalets Forskningspulje.

Declaration of conflicting interests

The author(s) declared no potential conflicts of interest with respect to the research, authorship, and/or publication of this article.

Authors' contributions

MBV, HKI and HBWL initiated and formulated the study. MBV, HKI, SAS, UL, UA and HBWL acquired the data. HKI, SAS, UA, SPC and HWBL performed the clinical evaluation of the patients. MBV and HBWL processed the data and performed the statistical analysis. MBV drafted the manuscript and prepared the figures. The remaining authors edited and revised the manuscript. All authors have approved the final version.

ORCID iD

Ulrich Lindberg https://orcid.org/0000-0002-0004-6354

References

1. Inzitari D, Eliasziw M, Gates P, et al. The causes and risk of stroke in patients with asymptomatic internal-carotid-artery stenosis. *N Engl J Med* 2000; 342: 1693–1700.
2. Yamauchi H, Kagawa S, Kishibe Y, et al. Misery perfusion, blood pressure control, and 5-year stroke risk in symptomatic major cerebral artery disease. *Stroke* 2015; 46: 265–268.
3. Yamauchi H, Fukuyama H, Nagahama Y, et al. Evidence of misery perfusion and risk for recurrent stroke in major cerebral arterial occlusive diseases from PET. *J Neurol Neurosurg Psychiatry* 1996; 61: 18–25.
4. Silvestrini M, Viticchi G, Falsetti L, et al. The role of carotid atherosclerosis in Alzheimer's disease progression. *J Alzheimers Dis* 2011; 25: 719–726.
5. Wendell CR, Waldstein SR, Ferrucci L, et al. Carotid atherosclerosis and prospective risk of dementia. *Stroke* 2012; 43: 3319–3324.
6. Baradaran H, Demissie S, Himali JJ, et al. The progression of carotid atherosclerosis and imaging markers of dementia. *Dement Transl Res Clin Interv* 2020; 6: 1–7.
7. Liu Z and Li Y. Cortical cerebral blood flow, oxygen extraction fraction, and metabolic rate in patients with Middle cerebral artery stenosis or acute stroke. *AJNR Am J Neuroradiol* 2016; 37: 607–614.
8. Yamauchi H, Higashi T, Kagawa S, et al. Is misery perfusion still a predictor of stroke in symptomatic major cerebral artery disease? *Brain* 2012; 135: 2515–2526.
9. Naylor AR, Ricco JB, de Borst GJ, et al. Management of atherosclerotic carotid and vertebral artery disease: 2017 clinical practice guidelines of the European Society for Vascular Surgery (ESVS). *Eur J Vasc Endovasc Surg* 2018; 55: 3–81.
10. Silvestrini M, Vernieri F, Pasqualetti P, et al. Impaired cerebral vasoreactivity and risk of stroke in patients with asymptomatic carotid artery stenosis mauro. *JAMA* 2000; 283: 2122–2127.
11. Reinhard M, Schwarzer G, Briel M, et al. Cerebrovascular reactivity predicts stroke in high-grade carotid artery disease. *Neurology* 2014; 83: 1424–1431.
12. Hino A, Tenjin H, Horikawa Y, et al. Hemodynamic and metabolic changes after carotid endarterectomy in patients with high-degree carotid artery stenosis. *J Stroke Cerebrovasc Dis* 2005; 14: 234–238.
13. Matsubara S, Moroi J, Suzuki A, et al. Analysis of cerebral perfusion and metabolism assessed with positron emission tomography before and after carotid artery stenting: clinical article. *J Neurosurg* 2009; 111: 28–36.
14. Leblanc R, Tyler JL, Mohr G, et al. Hemodynamic and metabolic effects of cerebral revascularization. *J Neurosurg* 1987; 66: 529–535.
15. Jespersen SN and Østergaard L. The roles of cerebral blood flow, capillary transit time heterogeneity, and oxygen tension in brain oxygenation and metabolism. *J Cereb Blood Flow Metab* 2012; 32: 264–277.
16. Kuschinsky W and Paulson OB. Capillary circulation in the brain. *Cerebrovasc Brain Metab Rev* 1992; 4: 261–286.
17. Angleys H, Østergaard L and Jespersen SN. The effects of capillary transit time heterogeneity (CTH) on brain oxygenation. *J Cereb Blood Flow Metab* 2015; 35: 806–817.
18. Hertz MM and Paulson OB. Transfer across the human blood-brain barrier: Evidence for capillary recruitment and for a paradox glucose permeability increase in hypocapnia. *Microvasc Res* 1982; 24: 364–376.
19. Crone C. The permeability of capillaries in various organs as determined by use of the 'indicator diffusion' method. *Acta Physiol Scand* 1963; 58: 292–305.
20. Østergaard L, Jespersen SN, Mouridsen K, et al. The role of the cerebral capillaries in acute ischemic stroke: the extended penumbra model. *J Cereb Blood Flow Metab* 2013; 33: 635–648.
21. Østergaard L. Blood flow, capillary transit times, and tissue oxygenation: the centennial of capillary recruitment. *J Appl Physiol (1985)* 2020; 129: 1413–1421.
22. Eskildsen SF, Gyldensted L, Nagenthiraja K, et al. Increased cortical capillary transit time heterogeneity in Alzheimer's disease: a DSC-MRI perfusion study. *Neurobiol Aging* 2017; 50: 107–118.
23. Østergaard L, Jespersen SN, Engedahl T, et al. Capillary dysfunction: its detection and causative role in dementias and stroke. *Curr Neurol Neurosci Rep* 2015; 15. doi:10.1007/s11910-015-0557-x.
24. Greijer AE and Van Der Wall E. The role of hypoxia inducible factor 1 (HIF-1) in hypoxia induced apoptosis. *J Clin Pathol* 2004; 57: 1009–1014.
25. Sendoel A and Hengartner MO. Apoptotic cell death under hypoxia. *Physiology (Bethesda)* 2014; 29: 168–176.
26. Richter C, Schweizer M, Cossarizza A, et al. Control of apoptosis by the cellular ATP level. *FEBS Lett* 1996; 378: 107–110.
27. Kaczmarz S, Göttler J, Petr J, et al. Hemodynamic impairments within individual watershed areas in asymptomatic carotid artery stenosis by multimodal MRI. *J Cereb Blood Flow Metab* 2021; 41: 380–396.
28. Larsson HBW, Vestergaard MB, Lindberg U, et al. Brain capillary transit time heterogeneity in healthy volunteers measured by dynamic contrast-enhanced T1-weighted perfusion MRI. *J Magn Reson Imaging* 2017; 45: 1809–1820.
29. Simonsen SA, West AS, Heiberg AV, et al. Is the TOAST classification suitable for use in personalized medicine in ischemic stroke? *JPM* 2022; 12: 496.

30. Fazekas F, Chawluk JB and Alavi A. MR signal abnormalities at 1.5 T in Alzheimer's dementia and normal aging. *Am J Neuroradiol* 1987; 8: 421–426.
31. Grant EG, Benson CB, Moneta GL, et al. Carotid artery stenosis: grayscale and doppler ultrasound diagnosis – society of radiologists in ultrasound consensus conference. *Ultrasound Q* 2003; 19: 190–198.
32. Hollander M, Bots ML, I, del Sol A, et al. Carotid plaques increase the risk of stroke and subtypes of cerebral infarction in asymptomatic elderly: the Rotterdam Study. *Circulation* 2002; 105: 2872–2877.
33. Bakker CJG, Hartkamp MJ and Mali WPTM. Measuring blood flow by nontriggered 2D phase-contrast MR angiography. *Magn Reson Imaging* 1996; 14: 609–614.
34. Vestergaard MB, Lindberg U, Aachmann-Andersen NJ, et al. Comparison of global cerebral blood flow measured by phase-contrast mapping MRI with 15O-H2O positron emission tomography. *J Magn Reson Imaging* 2017; 45: 692–699.
35. Jain V, Langham MC and Wehrli FW. MRI estimation of global brain oxygen consumption rate. *J Cereb Blood Flow Metab* 2010; 30: 1598–1607.
36. Tang C, Blatter DD and Parker DL. Accuracy of phase-contrast flow measurements in the presence of partial-volume effects. *J Magn Reson Imaging* 1993; 3: 377–385.
37. Peng S-L, Su P, Wang F-N, et al. Optimization of phase-contrast MRI for the quantification of whole-brain cerebral blood flow. *J Magn Reson Imaging* 2015; 42: 1126–1133.
38. Torack RM, Alcala H, Gado M, et al. Correlative assay of computerized cranial tomography (CCT), water content and specific gravity in normal and pathological postmortem brain. *J Neuropathol Exp Neurol* 1976; 35: 385–392.
39. Vestergaard MB and Larsson HBW. Cerebral metabolism and vascular reactivity during breath-hold and hypoxic challenge in freedivers and healthy controls. *J Cereb Blood Flow Metab* 2019; 39: 834–848.
40. Miao X, Nayak KS and Wood JC. In vivo validation of T2- and susceptibility-based SvO2 measurements with jugular vein catheterization under hypoxia and hypercapnia. *Magn Reson Med* 2019; 82: 2188–2198.
41. Larsson HBW, Courivaud F, Rostrup E, et al. Measurement of brain perfusion, blood volume, and blood-brain barrier permeability, using dynamic contrast-enhanced T1-weighted MRI at 3 tesla. *Magn Reson Med* 2009; 62: 1270–1281.
42. Schabel MC. A unified impulse response model for DCE-MRI. *Magn Reson Med* 2012; 68: 1632–1646.
43. Rasmussen PM, Jespersen SN and Østergaard L. The effects of transit time heterogeneity on brain oxygenation during rest and functional activation. *J Cereb Blood Flow Metab* 2015; 35: 432–442.
44. Jenkinson M, Beckmann CF, Behrens TEJ, et al. FSL. *Neuroimage* 2012; 62: 782–790.
45. Tatu L, Moulin T, Vuillier F, et al. Arterial territories of the human brain. *Front Neurol Neurosci* 2012; 30: 99–110.
46. Mutsaerts HJMM, Van Dalen J, Heijtel DFR, et al. Cerebral perfusion measurements in elderly with hypertension using arterial spin labeling. *PLoS One* 2015; 10: e0133717.
47. Hägerström D, Jakobsson D, Stomrud E, et al. A new automated method for analysis of rCBF-SPECT images based on the active-shape algorithm: normal values. *Clin Physiol Funct Imaging* 2012; 32: 114–119.
48. Edman Å, Edenbrandt L, Fredén-Lindqvist J, et al. Asymmetric cerebral blood flow in patients with mild cognitive impairment: possible relationship to further cognitive deterioration. *Dement Geriatr Cogn Dis Extra* 2011; 1: 228–236.
49. Chappell MA, Craig M and Woolrich MW. Stochastic variational bayesian inference for a nonlinear forward model. *arXiv* 2020; arXiv: 2007.01675.
50. Vagal AS, Leach JL, Fernandez-Ulloa M, et al. The acetazolamide challenge: techniques and applications in the evaluation of chronic cerebral ischemia. *AJNR Am J Neuroradiol* 2009; 30: 876–884.
51. Kuwabara Y, Ichiya Y, Sasaki M, et al. Time dependency of the acetazolamide effect on cerebral hemodynamics in patients with chronic occlusive cerebral arteries. *Stroke* 1995; 26: 1825–1829.
52. Watabe T, Shimosegawa E, Kato H, et al. Paradoxical reduction of cerebral blood flow after acetazolamide loading: a hemodynamic and metabolic study with 15O PET. *Neurosci Bull* 2014; 30: 845–856.
53. Fernández-Seara MA, Techawiboonwong A, Detre JA, et al. MR susceptometry for measuring global brain oxygen extraction. *Magn Reson Med* 2006; 55: 967–973.
54. Fernando MS, Simpson JE, Matthews F, et al. White matter lesions in an unselected cohort of the elderly: molecular pathology suggests origin from chronic hypoperfusion injury. *Stroke* 2006; 37: 1391–1398.
55. Stevenson SF, Doubal FN, Shuler K, et al. A systematic review of dynamic cerebral and peripheral endothelial function in lacunar stroke versus controls. *Stroke* 2010; 41: 434–442.
56. Hall CN, Reynell C, Gesslein B, et al. Capillary pericytes regulate cerebral blood flow in health and disease. *Nature* 2014; 508: 55–60.
57. Arsava EM, Hansen MB, Kaplan B, et al. The effect of carotid artery stenting on capillary transit time heterogeneity in patients with carotid artery stenosis. *Eur Stroke J* 2018; 3: 263–271.
58. Yamaguchi T, Kanno I, Uemura K, et al. Reduction in regional cerebral metabolic rate of oxygen during human aging. *Stroke* 1986; 17: 1220–1228.
59. Dalby RB, Eskildsen SF, Videbech P, et al. Oxygenation differs among white matter hyperintensities, intersected fiber tracts and unaffected white matter†. *Brain Commun* 2019; 1: fcz033. doi:10.1093/braincomms/fcz033.
60. Jiwa NS, Garrard P and Hainsworth AH. Experimental models of vascular dementia and vascular cognitive impairment: a systematic review. *J Neurochem* 2010; 115: 814–828.

61. Daulatzai MA. Cerebral hypoperfusion and glucose hypometabolism: key pathophysiological modulators promote neurodegeneration, cognitive impairment, and Alzheimer's disease. *J Neurosci Res* 2017; 95: 943–972.
62. Bennett SAL, Tenniswood M, Chen JH, et al. Chronic cerebral hypoperfusion elicits neuronal apoptosis and behavioral impairment. *Neuroreport* 1998; 9: 161–166.
63. Zonneveld HI, Loehrer EA, Hofman A, et al. The bidirectional association between reduced cerebral blood flow and brain atrophy in the general population. *J Cereb Blood Flow Metab* 2015; 35: 1882–1887.
64. Tomimoto H, Ihara M, Wakita H, et al. Chronic cerebral hypoperfusion induces white matter lesions and loss of oligodendroglia with DNA fragmentation in the rat. *Acta Neuropathol* 2003; 106: 527–534.
65. Zhang J, Liu T, Gupta A, et al. Quantitative mapping of cerebral metabolic rate of oxygen (CMRO2) using quantitative susceptibility mapping (QSM). *Magn Reson Med* 2015; 74: 945–952.
66. Puig O, Vestergaard MB, Lindberg U, et al. Phase contrast mapping MRI measurements of global cerebral blood flow across different perfusion states – a direct comparison with 15O-H2O positron emission tomography using a hybrid PET/MR system. *J Cereb Blood Flow Metab* 2019; 39: 2368–2378.
67. Ssali T, Anazodo UC, Thiessen JD, et al. A noninvasive method for quantifying cerebral blood flow by hybrid PET/MRI. *J Nucl Med* 2018; 59: 1329–1334.
68. Puig O, Henriksen OM, Vestergaard MB, et al. Comparison of simultaneous arterial spin labeling MRI and 15O-H2O PET measurements of regional cerebral blood flow in rest and altered perfusion states. *J Cereb Blood Flow Metab* 2020; 40: 1621–1633.
69. Zhang K, Herzog H, Mauler J, et al. Comparison of cerebral blood flow acquired by simultaneous [(15)O] water positron emission tomography and arterial spin labeling magnetic resonance imaging. *J Cereb Blood Flow Metab* 2014; 34: 1373–1380.